AUTOMATIC ROCKS DETECTION AND CLASSIFICATION ON HIGH RESOLUTION IMAGES OF PLANETARY SURFACES. A. Aboudan[1] , A. Pacifici[1], A. Murana[1], P. Allemand[2], G. G. Ori[1], A. Marcer[3], S. Portigliotti[3] and L. Lorenzoni[4], [1]Int'l Research School of Planetary Sciences, Università d'Annunzio, Viale Pindaro, 42, 65127 Pescara - Italy (aboudan@irsps.unich.it), [2]Université de Lyon, CNRS Université de Lyon1 et ENS-Lyon, [3]Thales Alenia Space - Italia, Business Segment Optical Observation and Science, Business Line Observation Exploration & Navigation, [4]European Space Research and Technology Centre ESTEC.

Introduction: This work describes a Rock Automated Detector (RAD) algorithm developed for the analysis of ExoMars 2016 mission landing site.

Rock Abundance (RA), rocks size-frequency distributions and cumulative area covered form rocks have been widely used to assess the landing risk for planetary probes on Mars [1][2][3][4]. Nevertheless this information is useful to understand the geologic history and evolution of planetary surfaces, evaluate the surface roughness and the degree of erosion/deposition that has occurred [5].

High-resolution images of planetary surfaces can be used to perform rock detection but manual searching for rocks is an intensive work even for small areas. As a consequence, an automatic or semi-automatic algorithm to identify rocks is mandatory to enable further processing as determining the rocks presence, size, height (by means of shadows) and spatial distribution over an area of interest.

The performances of this algorithm have been evaluated on both images of Martian analogue area of Morocco desert and HiRISE images. Results have been compared with ground truth obtained by means of manual rock identification. The experimental activity gave evidence that the developed algorithm is effective on isolated rocks as well on rocks clusters. Moreover this algorithm can be applied on images taken with very different illumination conditions and on terrains with a broad range of textures.

Method: rocks on high-resolution images appear to have a huge variety of textures and very often their Data Number (DN) is close to the image background. Moreover rocks can be clustered together in self-occluding piles and/or partially covered from sand. Image histograms are unimodal and bell-shaped with two tails corresponding to shadows on one side and rocks on the other.

The proposed algorithm uses morphological top-hat and bottom-hat operators to put in evidence the brighter and darkest pixel on the image.

Since both rocks and cast shadows can have different size, the image is processed using circular operators at different scales. Then, the corrected images are transformed in binary maps by means of maximum entropy thresholding [6][7]. Binary maps at different scales are combined and only the pixels classified over a minimum number of scales are retained.

Connected components are identified on the two maps (rocks and shadows).

Shadow are fitted with ellipses and, for each, ellipse, the corresponding rock footprint is defined as a circle, with the center on the shadow terminator and the radius computed as the projection of the ellipse on the direction orthogonal to the light (similar to [2][6]).

Finally rocks determined from shadows and rocks determined from image analysis are merged on a final rock map.

Validation on Mars analogue terrain: this algorithm has been validated by means of a imaging campaign on the Morocco desert. DRELIO drone has been used to get high-resolution images (up to 2 cm/px) of Mars analogue areas, and then the RAD has been used to map rocks and build rock abundance maps.

RAD results have been compared with manual mapped rocks on some selected sites/image crops. RAD was able to detect the 95% to 97% of rocks covered by at least 4 pixels.

The estimated RA ranges from 1% to 45%. Rock covered area resulted slightly overestimated for small rocks (4 to 12 pixels) and underestimated for isolated big rocks (more than 50 pixels). Putting some limit on the maximum size of rocks and on the maximum scale of morphological operators the error on the RA is limited to +- 5%.

Testing on HiRISE images: RAD has been tested also on HiRISE images of different terrains (even if not suitable for probes landing) and with different incidence angles.

For each image the rock abundance map, rock size-frequency distribution and rock height/diameter-frequency distribution have been computed. As an example results from PSP_013249_1270 are shown in the following figures.

Rocks size-frequency distributions decay following a power law (in the considered diameter ranges) consistently with fragmentation theories [8]. The distribution of rocks height/diameter ratio clusters between 0.5 and 0.75 (examples in Figure 1 and Figure 2).

The cumulative fractional area covered by rocks tends to converge (for diameter that goes to zero) to the mean observed rock abundance (example in Figure 3). Even if this characteristic curve is widely used to evaluate landing hazards it does not represent the spatial distribution of rocks. Locally the rock abundance

can exceed the observed mean of many orders of magnitude (example in Figure 4). Hence only the map of rock abundance (properly binned) can be used to properly identify the rockiest areas (hazards) and investigate deposition and transport phenomena that shaped the surface.

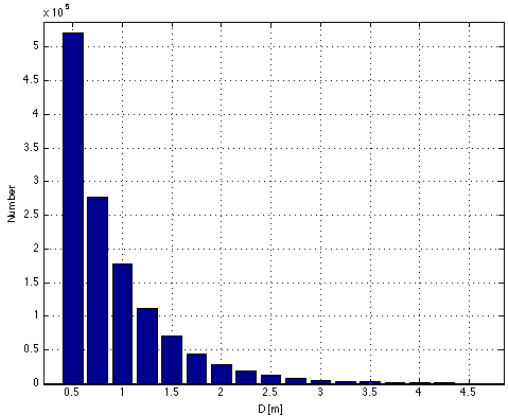

Figure 1: PSP_013249_1270 rocks size-frequency distribution.

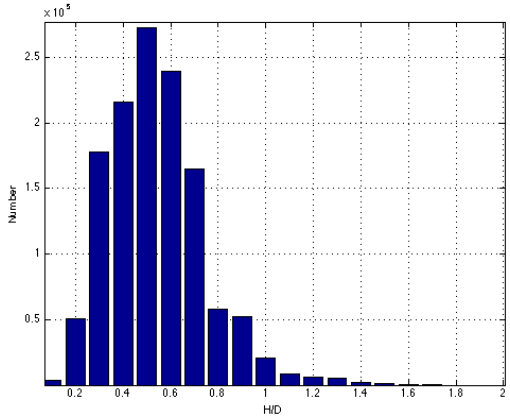

Figure 2: PSP_013249_1270 rocks height/diameter ratio frequency distribution.

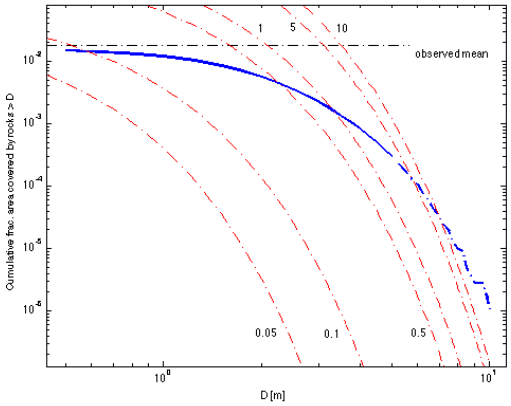

Figure 3: PSP_013249_1270 fractional cumulative area covered by rocks with diameter > D. The curve tends to the observed mean rock abundance of 1.7%. Red curves are the generalized models developed fitting Viking data for 0.05, 0.1, 0.5, 1, 5 and 10 total rock coverage [8].

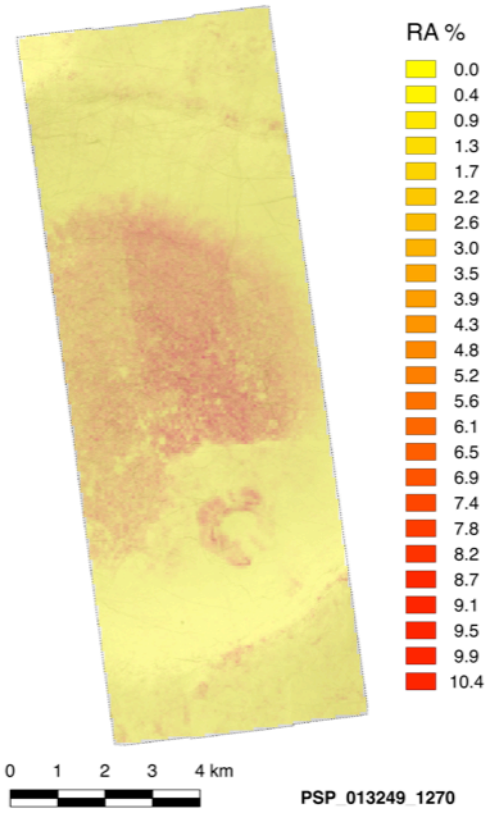

Figure 4: PSP_013249_1270 rock abundance map binned at 64 m. The observed mean rock abundance is 1.7% but locally the area covered by rocks can reach the 10% (red pixels).

References: [1] Golombek M. P. et al. (2003) *JGR, 108(E12),* 8086. [2] Golombek M. P. et al. (2008) JGR, *113,* E00A09. [3] Golombek M. P. et al. (2012) Mars 7, 1-22. [4] Golombek M. P. et al. (2011) LPSC XLII Abs. #1547 [5] Christensen P. R. (1986) *Icarus, 68, 217-238*. [6] Huertas A. et al. (2006) IEEE Aerospace Conf. Proc.. [7] Mehmet S. and Bulent S. (2004) Journal of Electronic Imaging, 13(1), 146-165. [8] Golombeck M. P. and Rapp D. (1997) JGR, 102(E2), 4117-4129.